ELSEVIER

Journal of Hazardous Materials B138 (2006) 471–478

Journal of Hazardous Materials

www.elsevier.com/locate/jhazmat

The effect of erbium on the adsorption and photodegradation of orange I in aqueous Er^{3+}-TiO_2 suspension

Chun-Hua Liang [a,c], Mei-Fang Hou [b], Shun-Gui Zhou [b], Fang-Bai Li [b,*], Cheng-Shuai Liu [b], Tong-Xu Liu [b], Yuan-Xue Gao [b], Xu-Gang Wang [a], Jia-Long Lü [a]

[a] *College of Resources and Environmental Sciences, Northwest Agriculture and Forestry University, Yangling, Shaanxi 712100, China*
[b] *Guangdong Key Laboratory of Agricultural Environment Pollution Integrated Control, Guangdong Institute of Eco-environment and Soil Sciences, Guangzhou 510650, China*
[c] *Department of chemistry, Huai Hua College, Huaihua, Hunan 418300, China*

Received 31 March 2006; received in revised form 23 May 2006; accepted 23 May 2006
Available online 2 June 2006

Abstract

Pure TiO_2 and erbium ion-doped TiO_2 (Er^{3+}-TiO_2) catalysts prepared by the sol–gel method were characterized by means of XRD and diffusive reflectance spectra (DRS). The XRD results showed that erbium ion doping could enhance the thermal stability of TiO_2 and inhibit the increase of the crystallite size, and the DRS results showed that the optical absorption edge slightly shifted to red direction owing to erbium ion doping and the Er^{3+}-TiO_2 catalysts had three typical absorption peaks located at 490, 523 and 654 nm owing to the transition of 4f electron from $^4I_{15/2}$ to $^4F_{7/2}$, $^2H_{11/2}$ and $^4F_{9/2}$. With a purpose of azo dyes degradation, orange I was used as a model chemical. And the adsorption isotherm, degradation and mineralization of orange I were investigated in aqueous suspension of pure TiO_2 or Er^{3+}-TiO_2 catalysts. The results showed that Er^{3+}-TiO_2 catalysts had higher adsorption equilibrium constants and better adsorption capacity than pure TiO_2. The adsorption equilibrium constants (K_a) of Er^{3+}-TiO_2 catalysts were about twice of that of pure TiO_2. The maximum adsorption capacity (Q_{max}) of 2.0% Er^{3+}-TiO_2 catalyst was 13.08×10^{-5} mol/g, which was much higher than that of pure TiO_2 with 9.03×10^{-5} mol/g. Among Er^{3+}-TiO_2 catalysts, 2.0% Er^{3+}-TiO_2 catalyst achieved the highest Q_{max} and K_a values. The kinetics of the orange I degradation using different Er^{3+}-TiO_2 catalysts were also studied. The results demonstrated that the degradation and mineralization of orange I under both UV radiation and visible light were more efficient with Er^{3+}-TiO_2 catalyst than with pure TiO_2, and an optimal dosage of erbium ion at 1.5% achieved the highest degradation rate. The higher photoactivity under visible light might be attributable to the transitions of 4f electrons of Er^{3+} and red shifts of the optical absorption edge of TiO_2 by erbium ion doping.

Keywords: Erbium; Photodegradation; Azo dye; Orange I; Ion doping; TiO_2

1. Introduction

Azo dyes wastewater has caused a primary environmental problem, not only because these dyes are relatively resistant to conventional treatment methods, but also because some of them produce carcinogenic amine as byproducts of hydrolysis [1,2]. In recent years, it has been is reported that TiO_2-based photocatalytic process should be a promising technique for the mineralization of azo dyes [3], since the other techniques, such as adsorption, combustion, wet oxidation and so on, had more or less disadvantages and they showed different degrees of cost effectiveness [4,5].

TiO_2-based photocatalytic process has been widely studied because TiO_2 can be excited by UV irradiation to generate charges leading to the produce of oxidative radicals, which can mineralize organic pollutants into carbon dioxide and water efficiently [3,6–9]. However, the modification of TiO_2 is necessary to enhance the efficiency of TiO_2 photocatalysis and to improve the photocatalytic activity of TiO_2 under solar or visible light [10–12]. Among different modifications, doped by rare earth ions or their oxides is an effective method [13,14]. Rare earth ions have strong complex ability to adsorb various organic pollutants and facilitate the degradation of organic pollutants [15]. Moreover, rare earth ions doping can reduce the crystallite size but increase the surface area of TiO_2, which also contribute to the enhancement of adsorption capacity of TiO_2 for organic pollutants [16,17]. It is reported that rare earth ions doping can lead

* Corresponding author. Tel.: +86 20 87024721; fax: +86 20 87024123.
E-mail address: cefbli@soil.gd.cn (F.-B. Li).

0304-3894/$ – see front matter © 2006 Elsevier B.V. All rights reserved.
doi:10.1016/j.jhazmat.2006.05.066

to the red shift of absorption edge of TiO_2, which is one of the ways to improve visible light photocatalytic activity of TiO_2 effectively [18]. The transitions of 4f electrons of rare earth ions can also improve photocatalytic activity of TiO_2 under irradiation of UV or visible light by increase of separating rate of photogenerated charges [19,20]. Thus, it is suggested that rare earth doping can provide TiO_2 with better adsorption abilities and better photocatalytic performances. Recently, erbium ion (Er^{3+}) attracted more attention in TiO_2-based optical materials [21–23], but it was less reported for photodegradation of organic pollutants [24]. Azo dyes are ordinary organic pollutants, among which orange II has been much studied. However, as the isomeric compound of orange II, orange I has been little studied in the photocatalytic process, especially its removal with photocatalytic process by erbium ion-doped TiO_2 (Er^{3+}-TiO_2) catalysts.

In present study, a series of erbium ion-doped titanium dioxide (Er^{3+}-TiO_2) catalysts were prepared by doping erbium ion into TiO_2 structure with different content by the sol–gel method. The adsorption, degradation and mineralization of orange I were investigated in aqueous suspension using the pure TiO_2 and erbium ion-doped TiO_2 (Er^{3+}-TiO_2) catalysts.

2. Experimental

2.1. Materials

Orange I was purchased from the special chemical corporation of Shanghai, China and used as received without further purification. Chemicals including tetra-*n*-butyl titanium [Ti(O-Bu)$_4$], Er(NO$_3$)$_3$, acetic acid (99.8%), absolute ethanol and ethanol (95%) were purchased from Aldrich and used as received.

2.2. Preparation of Er^{3+}-TiO_2 catalysts

A series of Er^{3+}-TiO_2 catalysts were prepared by the sol–gel method with the following procedure: firstly, 17 ml of tetra-*n*-butyl titanium [Ti(O-Bu)$_4$] was dissolved into 80 ml of absolute ethanol. And then the Ti(O-Bu)$_4$ solution was added drop-wise into 100 ml of the mixture solution containing 84 ml of ethanol (95%), 1 ml of 0.1 mol/l Er(NO$_3$)$_3$, and 15 ml of acetic acid (99.8%) under vigorous stirring, the resulting transparent colloidal suspension was stirred for 2 h before aged for 2 days for the formation of gel. The gel was dried at 353 K under vacuum and then ground into powder. The powder was calcined at 773 K for 2 h and the product Er^{3+}-TiO_2 powder catalyst was eventually obtained in a nominal atomic doping level of 0.5% as 0.5% Er^{3+}-TiO_2. Other Er^{3+}-TiO_2 samples were also prepared according to the above procedure as 1.0% Er^{3+}-TiO_2, 1.5% Er^{3+}-TiO_2, and 2.0% Er^{3+}-TiO_2. Pure TiO_2 was prepared without addition of Er(NO$_3$)$_3$ in the procedure.

2.3. Characterization of catalysts

To determine the crystal phase composition of the prepared TiO_2 and Er^{3+}-TiO_2 samples, X-ray diffraction (XRD) measurement was carried out at room temperature using a Rigaku D/MAX-IIIA diffractometer with Cu Kα ($\lambda = 0.15418$ nm) with the accelerating voltage of 30 kV and the emission current of 30 mA. To study the light absorption of the catalysts, the diffusive reflectance spectra (DRS) of the catalyst samples in the wavelength range of 200–900 nm were obtained using a UV–vis spectrophotometer (Shimadzu UV, 2101PC), with $BaSO_4$ as a reference.

2.4. Adsorption isotherm experiment

Adsorption is an indispensable step in any heterogeneous photocatalytic reaction. To investigate the adsorption behavior of pure TiO_2 and Er^{3+}-TiO_2 catalysts, a set of adsorption isotherm tests were performed in the dark. A fixed amount of the adsorbent (0.1 g) was added to 10 ml of orange I solution of varying concentrations taken in stoppered glass tubes, which were agitated for 24 h at 180 rpm in a thermostatic shaker bath and maintained at a temperature of $25 \pm 1\,^{\circ}C$ until equilibrium was reached. At time $t = 0$ and equilibrium, the orange I concentrations of the solutions were measured by UV–vis spectrometer and the adsorbed amount of orange I on pure TiO_2 or Er^{3+}-TiO_2 catalysts were calculated based on a mass balance.

2.5. Photoreactor system and experimental procedures

A Pyrex cylindrical photoreactor was used in the experiments, in which an 8-W medium-pressure mercury lamp with an emission peak at 365 nm (Westbury, New York) or a 70-W high-pressure sodium lamp (Shanghai, China) with main emission in the range of 400–800 nm was positioned at the centre of the cylindrical vessel and surrounded by a circulating water jacket to control the temperature at $25 \pm 1\,^{\circ}C$ during reaction. The reaction suspension was prepared by adding 0.25 g of photocatalyst powder into 250 ml of aqueous orange I solution. Prior to photocatalytic oxidation, the suspension was magnetically stirred in a dark condition for 30 min to establish adsorption/desorption equilibrium. The aqueous suspension containing orange I and photocatalyst was irradiated under UV or vis illumination with constant aeration. At the given time intervals, the analytical samples were taken from the suspension and immediately centrifuged at 4500 rpm for 20 min, then filtered through a 0.45 μm Millipore filter to remove the particles. The filtrate was stored in the dark for needed analysis.

2.6. Analytic method

To measure orange I concentration of centrifuged samples, a UV–vis spectrophotometer (UV–vis TU-1800, Purkinje General, Beijing) was used to determine the absorbance of orange I at a wavelength of 481 nm. The absorbance set at 481 nm is due to the color of the dye solution and it is used to monitor the degradation of dye. The total organic carbon (TOC) concentration was determined using a Total Organic Analyzer instrument (Shimadzu TOC-V CPH).

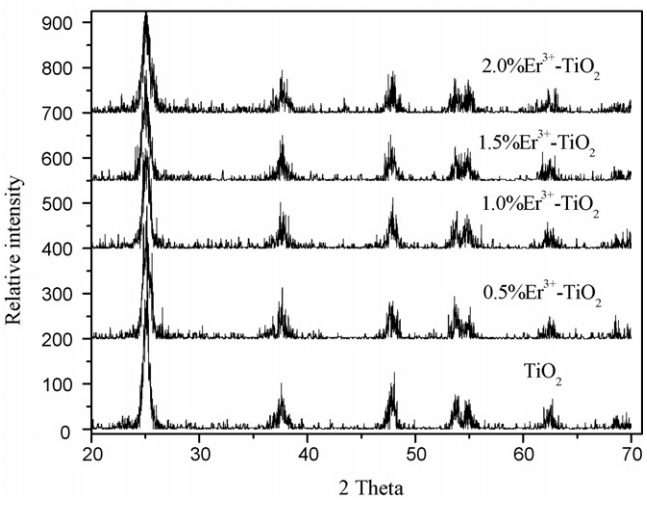

Fig. 1. The XRD patterns of pure TiO_2 and Er^{3+}-TiO_2 catalyst powders.

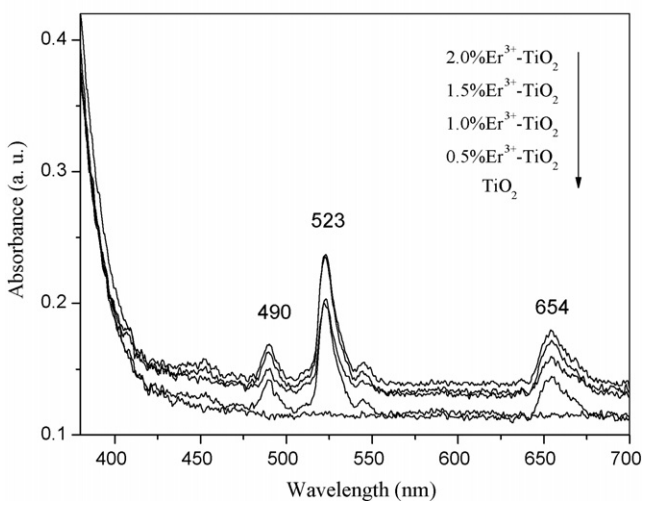

Fig. 2. The UV–vis diffuse reflectance spectra of TiO_2 and Er^{3+}-TiO_2 catalysts.

3. Results and discussion

3.1. X-ray diffraction

The crystal structure of pure TiO_2 and Er^{3+}-TiO_2 catalyst powders were analyzed by means of X-ray diffraction (XRD), as shown in Fig. 1. The results showed that all catalysts were dominated by anatase TiO_2 and the relative intensity of 101 peaks decreased significantly with the increase of erbium ion dosage. Based on the XRD data, the crystallite sizes of the Er^{3+}-TiO_2 samples were calculated by using the Scherrer formula, and the results showed that the crystallite size decreased with the increase of Er^{3+} dosage (Table 1), which indicated that erbium ion doping could inhibit the phase transformation of TiO_2 in the solid from anatase to rutile, lead to a higher thermal stability, and also could hinder the increase of the crystallite size. Smaller crystallite size would contribute to larger surface area. Jeon and Braun prepared Er^{3+}-doped luminescent TiO_2 nanoparticles for photonic applications by hydrothermal method with the sol–gel precursors, and it was found that erbium ion doping lead to a change in the morphology of nanoparticles from rod-like to triangular with the increase of the ratio of erbium ion to Ti from 1% to 3 mol%, resulting in inhibiting the growth of specific facets of the TiO_2 particles [25]. Thus, it can be deduced that erbium ion doping could enhance the thermal stability of anatase TiO_2, hinder the increase of its crystallite size and increase its surface area.

Table 1
Crystal parameters of different catalysts

	Er^{3+} doping content (mol/mol)				
	0.0%	0.5%	1.0%	1.5%	2.0%
Crystal structure	Anatase	Anatase	Anatase	Anatase	Anatase
Crystallite size (nm)	31.8	21.9	20.6	18.6	18.4
Lattice parameter, *a* (nm)	0.382	0.382	0.380	0.379	0.380
Lattice parameter, *c* (nm)	0.955	0.954	0.952	0.951	0.949

3.2. Diffusive reflectance spectra analysis

To study the optical absorption properties of catalysts, the diffusive reflectance spectra (DRS) in the range of 200–700 nm was investigated as shown in Fig. 2. The results showed that pure TiO_2 had no adsorption in the visible light region (>400 nm), while Er^{3+}-TiO_2 catalysts had three typical absorption peaks located at 490, 523 and 654 nm, corresponding to the transitions from $^4I_{15/2}$ to $^4F_{7/2}$, $^2H_{11/2}$ and $^4F_{9/2}$, respectively. According to Judd-Ofelt theory of parity-forbidden electric-dipole transitions of rare earth ions, the energy states of the Er^{3+} should be effectively perturbed by the odd terms of the Hamiltonian of the weak crystal field. Although 4f energy electrons have been partially screened by $5s^2$ and $5p^6$ electrons shells, the perturbations can still cause the permitted transitions of the 4f elections between 4f energy levels [26]. The transitions of 4f electrons of Er^{3+} favor the separation of photogenerated electron–hole pairs, the sensitization of TiO_2 by visible light and the complexation with azo dyes. The optical absorption edge shifted slightly to the red direction for Er^{3+}-TiO_2 catalysts. That is helpful to the improvement of photocatalytic activity under visible light. The transitions of 4f electrons of Er^{3+} and red shifts of the optical absorption edge of TiO_2 by erbium ion doping might lead to a higher photocatalytic activity under visible light.

3.3. Absorption isotherms

A set of adsorption experiments was carried out to determine the adsorption isotherms of orange I on pure TiO_2 and Er^{3+}-TiO_2 catalysts and the results were shown in Fig. 3(a). The adsorption isotherms of orange I can be analyzed by the following Langmuir adsorption model:

$$\theta = \frac{K_a C_e}{1 + K_a C_e} \quad (1)$$

where θ is the coverage of the organic substrate on the TiO_2 surface, C_e is the concentration of the substrate in the solution at equilibrium (mol/l), K_a is the Langmuir adsorption equilibrium

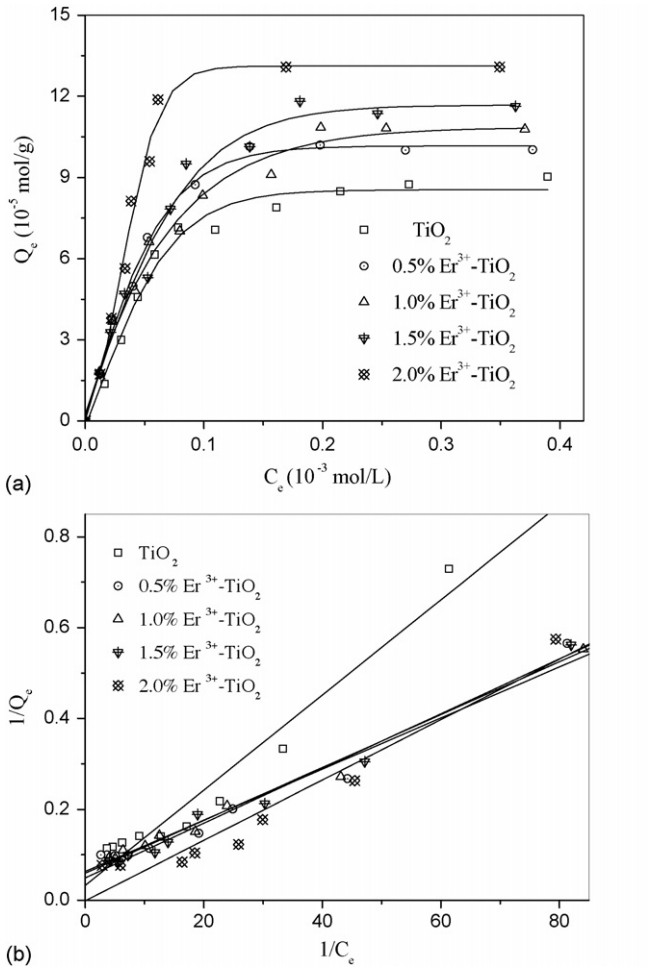

Fig. 3. Adsorption isotherms of orange I on pure TiO_2 and Er^{3+}-TiO_2 catalyst.

constant (l/mol). The coverage (θ) can be expressed as a ratio of the amount of the substrate adsorbed at equilibrium to the maximum amount adsorbed:

$$\theta = \frac{Q_e}{Q_{max}} \quad (2)$$

Combination and rearrangement of Eqs. (1) and (2) yields Eq. (3):

$$\frac{1}{Q_e} = \frac{1}{K_a Q_{max}} \frac{1}{C_e} + \frac{1}{Q_{max}} \quad (3)$$

The plot of $1/Q_e$ versus $1/C_e$ would obtain the straight line, as shown in Fig. 3(b), and then Q_{max} and K_a can be derived from the intercept and the slope of the plot. The correlation coefficient R represents the conformity between the experimental data and the Langmuir adsorption isotherm model. Based on the adsorption experimental data of orange I, K_a, Q_{max} and the correlation coefficient were obtained and shown in Table 2.

Table 2
The adsorption equilibrium constants (K_a) and the maximum adsorption amount (Q_{max}) of orange I on different catalyst

Photocatalysts	K_a ($\times 10^3$ l/mol)	Q_{max} ($\times 10^{-6}$ mol/g)	R^2
TiO_2	14.96	10.89	0.973
0.5% Er^{3+}-TiO_2	15.08	13.91	0.953
1.0% Er^{3+}-TiO_2	15.27	14.38	0.992
1.5% Er^{3+}-TiO_2	15.34	14.35	0.975
2.0% Er^{3+}-TiO_2	19.85	15.12	0.949

The results indicated that the adsorption equilibrium constants (K_a) of Er^{3+}-TiO_2 catalysts were about twice of that of pure TiO_2 catalyst. The maximum adsorption capacity of 2.0% Er^{3+}-TiO_2 catalyst was 13.08×10^{-5} mol/g, which was much higher than that of pure TiO_2 with 9.03×10^{-5} mol/g. Among Er^{3+}-TiO_2 catalysts, 2.0% Er^{3+}-TiO_2 catalyst achieved the highest Q_{max} and K_a values. The factors that led to the enhanced adsorption capacity should involve the change of the physical and chemical properties of the catalysts owing to erbium ion doping. The smaller crystal size and larger specific surface area of Er^{3+}-TiO_2 catalysts would be beneficial to better physical adsorption of orange I in the aqueous suspensions. Moreover, it had reported that Er^{3+} and other lanthanide ions can complex with azo dyes to form solid complexes [27,28]. Thus, there might be another important enhancement for the adsorption of orange I on Er^{3+}-TiO_2 by forming a chemical complex of Er^{3+} and orange I in the aqueous suspension.

3.4. Photocatalytic activity

The photocatalytic activities of pure TiO_2 and Er^{3+}-TiO_2 catalysts were examined by the photodegradation (decolorization) of orange I under UV light and visible light irradiation. The degradation kinetics of orange I on different catalysts under UV light and visible light could be analyzed by the pseudo-first-order kinetic model. On the basis of the experimental data, the plots of (C_t/C_0) versus t were shown in Fig. 4. The pseudo-first-order kinetic rate constants k_{ap} were listed in Table 3. It was shown that the photocatalytic activity of erbium ion-doped TiO_2 was significantly higher than that of pure TiO_2 under both UV light and visible light. The photocatalytic activity of TiO_2-based

Table 3
Pseudo-first-order kinetic constants of orange I degradation under UV light and visible light irradiation

	TiO_2	0.5% Er^{3+}-TiO_2	1.0% Er^{3+}-TiO_2	1.5% Er^{3+}-TiO_2	2.0% Er^{3+}-TiO_2
UV light					
k_{ap} (1/min)	0.0245	0.0328	0.0438	0.0683	0.0405
R^2	0.989	0.994	0.987	0.992	0.982
Visible light					
k_{ap} (1/min)	0.0155	0.0181	0.0219	0.0292	0.0204
R^2	0.992	0.998	0.999	0.999	0.988

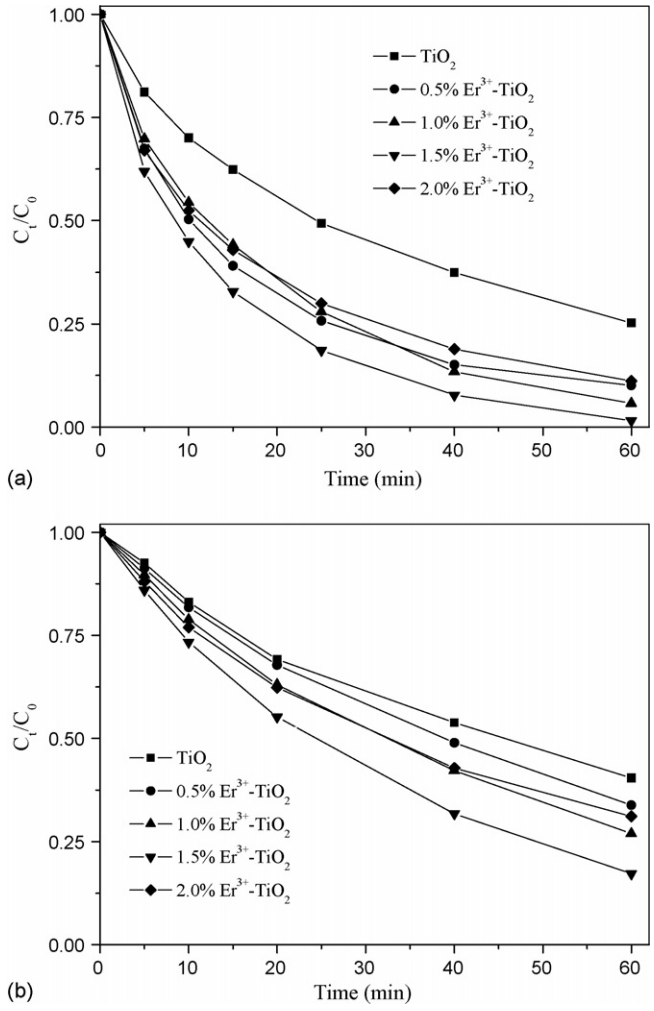

Fig. 4. The degradation of 6×10^{-5} mol/l orange I under UV light (a) and visible light irradiation (b) (pH 7.0, catalyst dosage: 1.0 g/l).

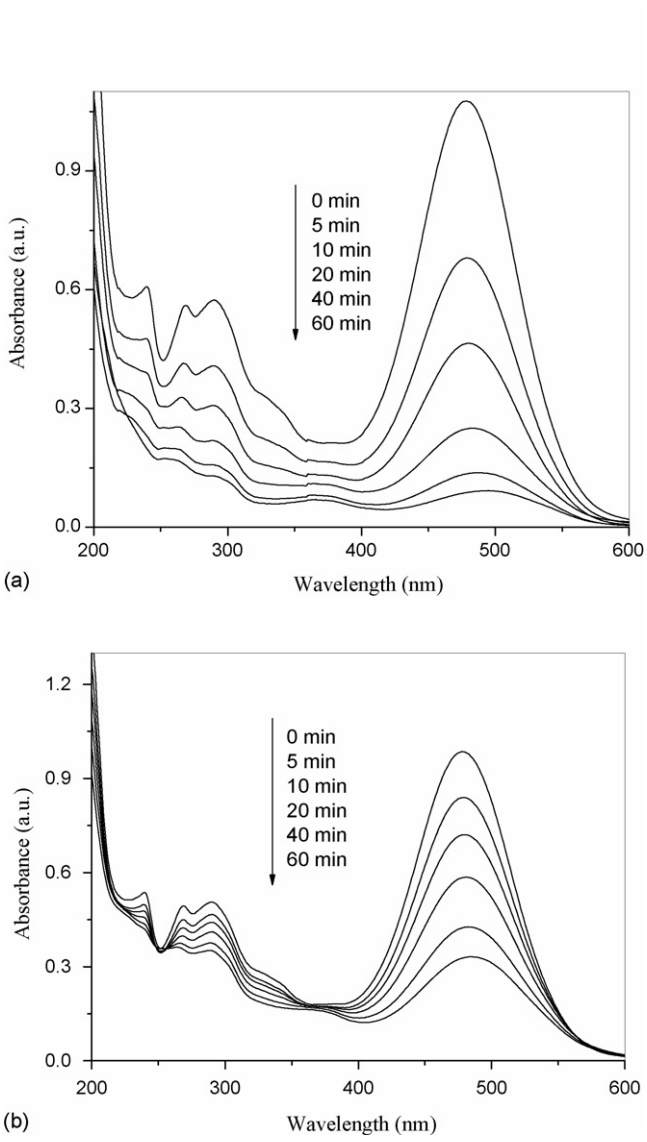

Fig. 5. The changes of UV–vis adsorption spectra of orange I solution (5.2×10^{-5} mol/l) on 1.5% Er^{3+}-TiO_2 under UV light (a) and visible light irradiation (b) (pH 7.0, catalyst dosage: 1.0 g/l).

catalysts increased with increasing the Er^{3+} doping dosage initially, but decreased when Er^{3+} doping content was over 1.5% under both UV light and visible light. 1.5% Er^{3+}-TiO_2 achieved the best photocatalytic performance under both UV light and visible light. Under visible light, orange I can be excited and an excited electron is generated. Then the excited electron can be transformed to TiO_2, then to O_2, and $O_2^{\bullet -}$ and hydroxyl radical are generated, as described by Eqs. (4)–(9). Therefore, pure TiO_2 should have photocatalytic activity owing to dye sensitization.

$$\text{dye} + h\nu \rightarrow \text{dye}^* \quad (4)$$

$$TiO_2 + \text{dye}^* \rightarrow TiO_2(e^-) + \text{dye}^{\bullet +} \quad (5)$$

$$O_2 + TiO_2(e^-) \rightarrow O_2^{\bullet -} + TiO_2 \quad (6)$$

$$O_2^{\bullet -} + H_2O \rightarrow HO_2^{\bullet} + OH^- \quad (7)$$

$$HO_2^{\bullet} + H_2O + TiO_2(e^-) \rightarrow H_2O_2 + OH^- + TiO_2 \quad (8)$$

$$H_2O_2 + TiO_2(e^-) \rightarrow OH^{\bullet} + OH^- + TiO_2 \quad (9)$$

It was also noted that the visible light irradiated photocatalytic activity of Er^{3+}-TiO_2 was near twice as much as that of pure TiO_2, and the UV irradiated photocatalytic activity of Er^{3+}-TiO_2 was near threefold as much as that of pure TiO_2. The photocatalytic activity of Er^{3+}-TiO_2 under visible light might be attributed to erbium ion doping, since erbium ion can lead to the red shifts of optical adsorption edges [18] and the enhancement of the overall up-conversion luminescence intensity [29]. Fig. 5(a) and (b) also showed that the changes in the optical densities of 481 nm (–N=N–), 290 nm (naphthalene ring) and 240 nm (benzene ring) of orange I under different illumination time under UV light and visible light. Obviously, three adsorption peaks of orange I became weaker and weaker along with the illumination time. That indicated that both azo bonds and aromatic part of the dye molecule were attacked under both UV light and visible light. Thus, it can be deduced that erbium ion

doping can enhance the photocatalytic activity for the mineralization of orange I.

To further investigate the photocatalytic kinetics, the significant adsorption of orange I on the Er^{3+}-TiO_2 catalysts need to be considered. As known from the adsorption experimental data, the adsorption of orange I onto Er^{3+}-TiO_2 catalysts was obviously more than that of pure TiO_2. To describe the degradation kinetics of some substrates adsorbed on the TiO_2-based catalysts, the Langmuir–Hinshelwood (L–H) equation was usually used [30,31]. In fact, the L–H model has been established on the basis of Langmuir adsorption of the organic substrate onto the photocatalyst. Thus, the substrate adsorption has already been included in the L–H model whether the adsorption is strong or weak [31]. The L–H model can be expressed as follows:

$$-\frac{dC}{dt} = k_r \frac{K_a C}{1 + K_a C} \tag{10}$$

where $-dC/dt$ is the photocatalytic degradation rate in mol/(l min), k_r is the degradation kinetic constant also in mol/(l min), t is the reaction time in min, C is the concentration of orange I (mol/l) at time t and K_a is the adsorption equilibrium constants as same as in Eq. (1). If the product value of C and K_a is significantly smaller than 1, Eq. (10) may be simplified to pseudo-first-order kinetic equation as follows:

$$-\frac{dC}{dt} = k_r K_a C \tag{11}$$

Consequently an integrated form of Eq. (11) can be expressed as:

$$-\ln\left(\frac{C}{C_0}\right) = k_r K_a t \tag{12}$$

In this work, the initial concentration (C_0) of orange I was around 5.2×10^{-5} mol/l, the products of $K_a C_0$ were calculated to be between 0.78 and 1.03 which were not significant smaller than 1. So it should not be neglected. Under this situation, an integral form of the L–H model would be more feasible which can be expressed as below:

$$\ln\left(\frac{C_0}{C}\right) + K_a(C_0 - C) = k_r K_a t \tag{13}$$

Eq. (13) also can be rearranged as follows:

$$\ln\left(\frac{C_0}{C}\right) + K_a(C_0 - C) = k_{ap} t \tag{14}$$

where $k_{ap} = k_r K_a$, and it is the apparent kinetic constant in 1/min. The k_{ap} value can be obtained by plotting $\ln(C_0/C) + K_a(C_0 - C)$ versus t.

Obtained from the adsorption equilibrium coefficients (K_a) and the apparent kinetic constants (k_{ap}), the degradation kinetic constants (k_r) on pure TiO_2 and Er^{3+}-TiO_2 catalysts irradiated by UV light and visible light were shown in Fig. 6. The correlation coefficients with the L–H model were much better than those with the pseudo-first-order kinetic equation, which suggested that the adsorption plays an important role in the degradation of orange I on Er^{3+}-TiO_2. Similar to the pseudo-first-order kinetic

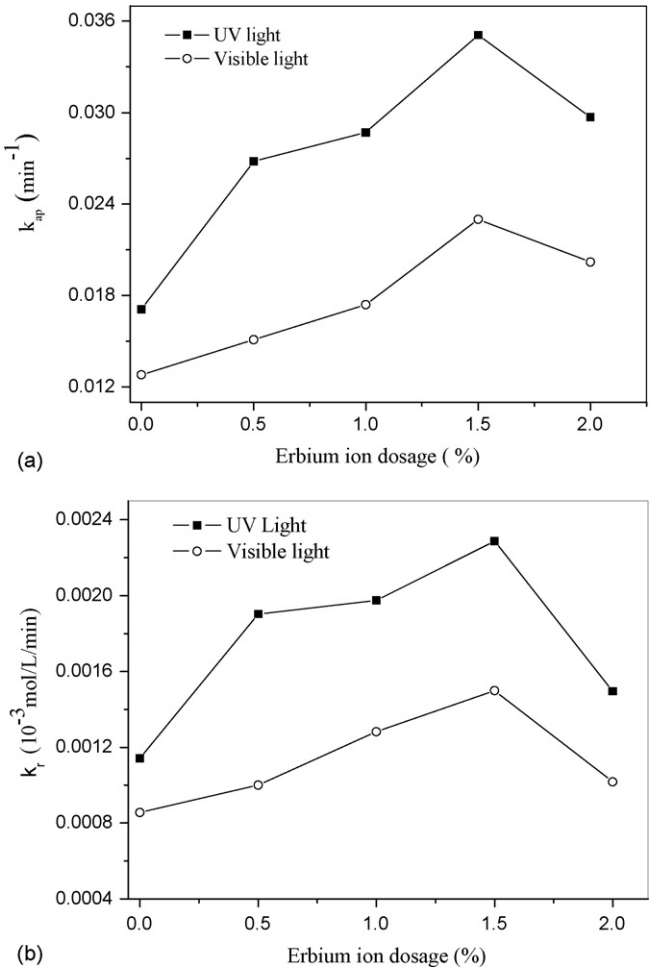

Fig. 6. Apparent kinetic constant k_{ap} (a) and kinetic constant k_r (b) of orange I photodegradation by using Er^{3+}-TiO_2 catalyst under UV light and visible light irradiation.

constants, the degradation kinetic constants (k_r) increased with the increase of Er^{3+} doping dosage initially, but decreased when Er^{3+} content is over 1.5%. It can be confirmed that 1.5% Er^{3+}-TiO_2 would achieve the best photocatalytic activity under both UV light and visible light.

3.5. Mineralization of orange I

Fig. 7 shows the TOC removal for orange I degradation after 120 min under UV light irradiation with different catalysts. The result showed that orange I was efficiently mineralized. The percentage of TOC removal was 65.4%, 74.0%, 75.4%, 64.0%, and 61.0%, respectively, in the suspension of pure TiO_2, and 0.5%, 1.0%, 1.5%, 2.0% Er^{3+}-TiO_2. The percentage of TOC removal of TiO_2-based catalysts increased with the increase of Er^{3+} doping dosage initially, but decreased when Er^{3+} content was over 1.0%. Obviously, 1.0% Er^{3+}-TiO_2 had the best performance for TOC removal, which was not consistent with that of the photocatalytic activity for orange I degradation, because the TOC removal was attributable to the mineralization of orange I, while the photocatalytic degradation for orange I was attributable to

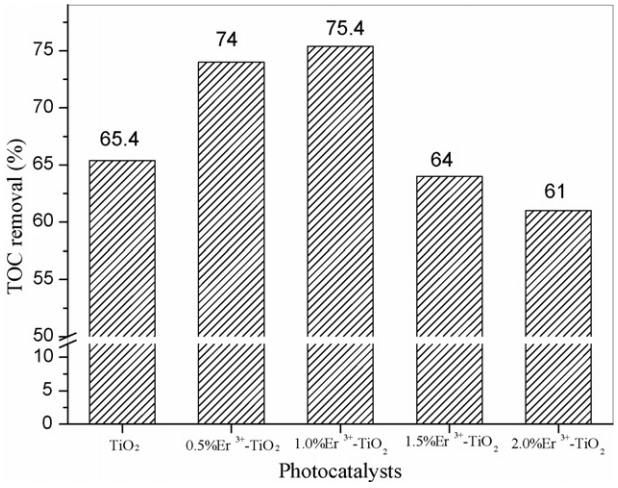

Fig. 7. TOC removal percentage of 6×10^{-5} mol/l orange I solution using 1.0 g/l different photocatalysts after 120 min under UV light irradiation.

the decolorization for the destroy of –N=N– in the molecular of orange I.

3.6. Discussion

The DRS spectra of Er^{3+}-doped TiO_2 catalysts showed that there were optical adsorption in visible region and slightly red shifts in the doped catalysts, which is ascribed to the transitions of 4f electrons of Er^{3+} from $^4I_{15/2}$ to $^4F_{7/2}$, $^2H_{11/2}$ and $^4F_{9/2}$, respectively. The transitions of 4f electrons of Er^{3+} favored the formation of photogenerated electron–hole pairs.

It is well known that the high photocatalytic activity of photocatalysts strongly depends on the better adsorption of organic substrate and the improvement of the interfacial charge-transfer reaction. On one hand, from the above results it can be concluded that the larger surface area, the smaller crystallite size and the Er^{3+} complex effect of the Er^{3+}-TiO_2 catalysts are favorable to the better adsorption of orange I, which benefits to the degradation of orange I. Furthermore, it was reported that the pairing effect between the ion-dopants led to the appearance of a solid solution in Er^{3+}-doped TiO_2 sol–gel layer [32]. Erbium ion doping might be more favorable to the separation of photoinduced electron–hole pairs, which would lead to the enhancement of photocatalytic activity [33].

The optimal dosage of erbium ion doping at 1.5% may be due to the fact that there was an optimal dosage of erbium ions in TiO_2 particles for the most efficient separation of photoinduced electron–hole pairs. With the concentration of doped ions increases, the surface barrier becomes higher, and the space charge region becomes narrower. So the electron–hole pairs within the region are efficiently separated by the large electric field. Moreover, when the concentration of doped ions is excessively high, the space charge region becomes very narrow and the penetration depth of light into TiO_2 greatly exceeds the space charge layer; therefore the recombination of the photogenerated electron–hole pairs becomes easier. Thus, there is an optimal Er^{3+} dosage for degradation of orange I.

4. Conclusion

Erbium ion doping could stabilize thermally anatase phase of TiO_2 and inhibit the increase of the crystallite size, and also improve the adsorption of orange I on TiO_2 significantly. The degradation of orange I under UV light and visible light radiation was better with Er^{3+}-TiO_2 catalyst than with pure TiO_2, and the optimal dosage of erbium ion was 1.5% under both UV radiation and visible light. Er^{3+}-TiO_2 could mineralize orange I more effectively than pure TiO_2. The separation efficiency of interfacial charges by Er^{3+} doping may lead to an optimal Er^{3+} dosage for the degradation of orange I. The transitions of 4f electrons of Er^{3+} and the red shift of the optical absorption edge of TiO_2 by Er^{3+} doping were useful to enhance photocatalytic activity under visible light.

Acknowledgements

The authors wish to thank the National Natural Scientific Foundation of China (20203007) and Guangdong Technological Foundation (2005B10301001) for financial supports to this work.

References

[1] A.S. Özen, V. Aviyente, G. Tezcanli-Güyer, N.H. Ince, Experimental and modeling approach to decolorization of azo dyes by ultrasound: degradation of the hydrazone tautomer, J. Phys. Chem. A 109 (2005) 3506–3516.
[2] M.S. Lucas, J.A. Peres, Decolorization of the azo dye reactive Black 5 by Fenton and photo-Fenton oxidation, Dyes Pigments 71 (2006) 236–244.
[3] V.V. Alexandre, Y.Ch. Chen, G.S. Panagiotis, Photocatalytic decolourisation and degradation of reactive orange 4 by TiO_2-UV process, J. Hazard. Mater. 113 (2004) 89–95.
[4] B. Neppolian, H.C. Choi, S. Sakthivel, B. Arabindoo, V. Murugesan, Comparison of the adsorption characteristics of azo-reactive dyes on mezoporous minerals, J. Hazard. Mater. 89 (2002) 303–317.
[5] K. Erdal, I.H. Sibel, Y. Ibrahim, S. Ali, E. Oktay, Comparison of the treatment methods efficiency for decolorization mineralization of Reactive Black 5 azo dye, J. Hazard. Mater. 119 (2005) 109–116.
[6] A.L. Linsebiger, G.Q. Lu Jr., J.T. Yates, Photocatalysis on TiO_2 surfaces: principles, mechanisms, and selected results, Chem. Rev. 95 (1995) 735–758.
[7] M.R. Hoffman, S.T. Martin, W. Choi, D.W. Bahnemann, Environmental applications of semiconductor photocatalysis, Chem. Rev. 95 (1995) 69–96.
[8] J.G. Yu, J.C. Yu, B. Cheng, S.K. Hark, K. Iu, The effect of F^--doping and temperature on the structural and textural evolution of mesoporous TiO_2 powders, J. Solid State Chem. 174 (2003) 372–380.
[9] J.G. Yu, J.C. Yu, B. Cheng, X.J. Zhao, Photocatalytic activity and characterization of the sol–gel derived Pb-doped TiO_2 thin films, J. Sol–Gel Sci. Technol. 24 (2002) 39–48.
[10] J.G. Yu, J.C. Yu, M.K.P. Leung, W.K. Ho, B. Cheng, X.J. Zhao, J.C. Zhao, Effects of acidic and basic hydrolysis catalysts on the photocatalytic activity and microstructures of bimodal mesoporous titania, J. Catal. 217 (2003) 69–78.
[11] Y.B. Xie, C.W. Yuan, Photocatalysis of neodymium ion modified TiO_2 sol under visible light irradiation, Appl. Surf. Sci. 221 (2004) 17–24.
[12] K.T. Ranjit, I. Willner, S.H. Bossmann, A.M. Braun, Lanthanide oxide-doped titanium dioxide photocatalysts: effective photocatalysts for the enhanced degradation of salicylic acid and *t*-cinnamic acid, J. Catal. 204 (2001) 305–311.
[13] F.B. Li, X.Z. Li, M.F. Hou, Photocatalytic degradation of 2-mercaptobenzothiazole in aqueous La^{3+}-TiO_2 suspension for odor control, Appl. Catal. B: Environ. 48 (2004) 185–194.

[14] F.B. Li, X.Z. Li, M.F. Hou, K.W. Cheah, W.C.H. Choy, Enhanced photocatalytic activity of Ce^{3+}-TiO_2 for 2-mercaptobenzothiazole degradation in aqueous suspension for odour control, Appl. Catal. A: Gen. 285 (2005) 181–189.
[15] K.T. Ranjit, I. Willner, S.H. Bossmann, A.M. Braun, Lanthanide oxide-doped titanium dioxide: effective photocatalysts for the degradation of organic pollutants, J. Mater. Sci. 34 (1999) 5273–5280.
[16] Y.H. Zhang, H.X. Zhang, Y.X. Xu, Y.G. Wang, Significant effect of lanthanide doping on the texture and properties of nanocrystalline mesoporous TiO_2, J. Solid State Chem. 177 (2004) 3490–3498.
[17] K.T. Ranjit, I. Willner, S.H. Bossmann, A.M. Braun, Lanthanide oxide-doped titanium dioxide photocatalysts: novel photocatalysts for the enhanced degradation of *p*-chlorophenoxyacetic acid, Environ. Sci. Technol. 35 (2001) 1544–1549.
[18] W. Xu, Y. Gao, H.Q. Liu, The preparation, characterization, and their photocatalytic activities of rare-earth-doped TiO_2 nanoparticles, J. Catal. 207 (2002) 151–157.
[19] Y.B. Xie, C.W. Yuan, X.Z. Li, Photocatalytic degradation of X-3B dye by visible light using lanthanide ion modified titanium dioxide hydrosol system, Colloid Surf. A: Physicochem. Eng. Aspects 252 (2005) 87–94.
[20] J. Lin, J.C. Yu, An investigation on photocatalytic activities of mixed TiO_2-rare earth oxides for the oxidation of acetone in air, J. Photochem. Photobiol. A: Chem. 116 (1998) 63–67.
[21] A. Bahtat, M. Bouazaoui, M. Bahtat, C. Garapon, B. Jacquier, J. Mugnier, Up-conversion fluorescence spectroscopy in Er^{3+}:TiO_2 planar waveguides prepared by a sol–gel process, J. Non-crystall. Solids 202 (1996) 16–22.
[22] Y.L. Huang, H.J. Seo, Y. Yang, J. Zhang, Visible up-conversion luminescence in Er^{3+}-doped $PbWO_4$ single crystals, Mater. Chem. Phys. 91 (2005) 424–430.
[23] S.X. Dai, J.L. Wu, J.J. Zhang, G.N. Wang, Z.H. Jiang, The spectroscopic properties of Er^{3+}-doped TeO_2–Nb_2O_5 glasses with high mechanical strength performance, Spectrochim. Acta Part A 62 (2005) 431–437.
[24] C. Mignotte, EXAFS studies on erbium-doped TiO_2 and ZrO_2 sol–gel thin films, J. Non-crystall. Solids 291 (2001) 56–77.
[25] S. Jeon, P.V. Braun, Hydrothermal synthesis of Er-doped luminescent TiO_2 nanoparticles, Chem. Mater. 15 (2003) 1256–1263.
[26] R. Guo, Y.C. Wu, P.Z. Fu, F.L. Jing, Optical transition probabilities of Er^{3+} ions $La_2CaB_{10}O_{19}$ crystal, Chem. Phys. Lett. 416 (2005) 133–136.
[27] N.T. Abdel-Ghani, A.L. El-Ansary, A.A. Salem, Thermogravimetric, potentiometric, conductimetric and spectrometric studies on lanthanide complexes with some hydroxynaphthoic acid azo dyes, Thermochim. Acta 122 (1987) 231–243.
[28] N.T. Abdel-Ghani, Y.M. Issa, A.A. Salem, Spectrophotometric determination of some lanthanides using 3-hydroxy-2-naphthoic acid azo dyes, Microchem. J. 39 (1989) 283–288.
[29] A. Patra, C.S. Friend, R. Kapoor, P.N. Prasad, Fluorescence upconversion properties of Er^{3+}-doped TiO_2 and $BaTiO_3$ nanocrystallites, Chem. Mater. 15 (2003) 3650–3655.
[30] A.P. Toor, A. Verma, C.K. Jotshi, P.K. Bajpai, V. Singh, Photocatalytic degradation of Direct Yellow 12 dye using UV/TiO_2 in a shallow pond slurry reactor, Dyes Pigments 68 (2006) 53–60.
[31] E. Evgenidou, K. Fytianos, I. Poulios, Semiconductor-sensitized photodegradation of dichlorvos in water using TiO_2 and ZnO as catalysts, Appl. Catal. B: Environ. 59 (2005) 81–89.
[32] C. Mignotte, EXAFS studies on erbium-doped TiO_2 and ZrO_2 sol–gel thin films, J. Non-crystall. Solids 291 (2001) 56–77.
[33] Q. Fang, M. Meier, J.J. Yu, Z.M. Wang, J.Y. Zhang, J.X. Wu, A. Kenyon, P. Hoffmann, W. Boyd Ian, FTIR and XPS investigation of Er-doped SiO_2-TiO_2 films, Mater. Sci. Eng. B 105 (2003) 209–213.